Songklanakarin J. Sci. Technol.
44 (2), 393-400, Mar. - Apr. 2022

http://www.sjst.psu.ac.th

Original Article

Mechanisms and mechanics of bonding in 3D printed materials systems based on traditional mould materials

Solaman B. Selvaraj[1*], and Sarat Singamneni[2]

[1] *Additive Manufacturing Lab, Vellore Institute of Technology, Vellore, 632014 India*

[2] *Additive Manufacturing Research Centre, Auckland University of Technology, Auckland, 1010 New Zealand*

Received: 21 July 2021; Revised: 14 September 2021; Accepted: 20 September 2021

Abstract

Common material systems used for 3D printing of sand-casting moulds are often plaster-based sand compositions with typical limitations. Bentonite-based sand composites and associated binding mechanisms are well established in traditional foundry practices, but possible use of similar systems is scarce in 3D printing. The current research attempts this, considering bentonite-sand composites of varying compositions for 3D printing and evaluating the mechanisms and mechanics of bonding. Differing amounts of α-hemihydrate together with varying quantities of terra alba as the seeding agent are identified to be effective together with impregnation by sodium silicate and subsequent baking at suitable temperatures. The bonding in green state is achieved through gypsum crystallisation and assisted by terra alba as the seeding component. Sodium silicate soaking and impregnation increased the compressive strength notably (1.3MPa) from green (0.49MPa) and directly baked without sodium silicate impregnation (0.19), with almost 2.7 fold increase from the green compressive strength and 7 fold from the directly dried case.

Keywords: 3D printing, bonding, mechanisms, mechanics, sodium silicate

1. Introduction

Additive manufacturing and 3D printing took long strides in the recent past and gradually evolved into alternative approaches for direct production of end use parts in some cases, and into possible means of expediting critical process steps in some other cases. While the chronology emerges as rapid prototyping, tooling, manufacturing, and currently additive manufacturing, the rapid tooling applications are by far the most successful in resolving the time-to market aspects of the traditional manufacturing methods. In casting, this was achieved by means of rapid prototyped wax patterns for investment casting (Lee, Chua, Cheah, Tan & Feng, 2004) direct production of injection moulding dies through laser sintering (Chua, Feng, Lee & Ang, 2005; Kent 1991) or direct metal laser sintering (Simchi Petzoldt & Pohl, 2003), and pattern-less production of sand moulds by laser sintering (Chhabra & Singh, 2011b; Rosochowski & Matuszak, 2000) or 3D printing (Chhabra & Singh, 2012, 2011b). Of all these approaches, the 3D printing of ceramic moulds has application potential for the benefit of small to medium scale foundries (Chhabra & Singh, 2011b). 3D printing refers to the Binder Jetting (BJ) process, unfortunately all other additive manufacturing processes are also called 3D printing. Binder jetting printer has three chambers, first for to store the candidate powder, second one is build chamber, and the third chamber is to collect the excess powder. A roller or recoater blade spreads the powder on the build chamber and print head deposits liquid binder selectively as per the profile of the part. Bonding takes place by chemical reaction. (Mohammad Reza Khosravani & Tamara Reinicke, 2020).

In a commercial 3D printing system, the powder mixture is spread as thin layers on a substrate and aqueous glue is delivered through the ink-jet nozzle to consolidate the powder particles selectively through a drop-on-demand system (Bredt, Anderson & Russell, 2002). The crystals grow into the inter-granular spaces between the sand particles and hold the substrate with sufficient green strength (Singh &

*Corresponding author
Email address: ssolomanbobby@vit.ac.in

Middendorf, 2007). According to the theory of dehydration, the subsequent baking process first results in the formation of hemihydrate and beyond 350^0C anhydrite crystals, as all the moisture is driven off and the dry strength is reduced to varying degrees (Mandal & Mandal 2002; Strydom, Hudson & Potgieter, 1995).

The accuracy and surface finish were reported to be similar to the results expected of traditional sand casting (Bak, 2003). Dorinka, Beloy and Chekhonin (2011) evaluated the minimum shell thickness and calcination effects of moulds produced using Z-Cast while casting an aluminium alloy. While the strength of the moulds decreased with decreasing mould wall thickness, the calcination process was found to have detrimental effects on the printed sand moulds. A comparative study of the performance of different grades of powders available from Z-Corporation, undertaken by Gill and Kaplas (Gill & Kaplas, 2010) allowed to record varied performances with different metals, while in most cases, the investment casting results were better in terms of surface quality measures. Evidently, the science of material consolidation in 3D printing achieved very little research attention apart from the descriptions in the patent documents. Utela, Anderson and Ganter (2008) also noted that the material options are limited for 3D printing, often hindering wider applications, in spite of the benefits noted above. While the process development steps for new materials include powder, binder, and glue systems selection and development, complex and dynamic interactions are involved. Koltygin and Bazhenov (2012) had mould material properties were experimentally evaluated. The printed moulds were post-processed, impregnating with certain inorganic binders to increase the mould hardness (Markowski *et al*., 2010). While the casting material option from Z-Corp is apparently discontinued, Voxel Jet and ExOne have different new material systems to offer. Again, these are proprietary material systems, expensive, and research and scientific understanding of the underlying principles is scarcely explored and reported.

With traditional sand-casting processes on the other hand, the mould material ingredients, compositions, and mechanisms and mechanics of bonding are relatively well established. Traditional sand moulds are typically composed of 80% silica sand, 5-10% clay binders such as bentonite in majority cases, and 2-6% tempering water, as noted by Boylu (2011). The component that controls the binding attributes is montmorillonite, which swells with the addition of water, allowing colloidal and mechanical properties to develop for moulding sands (Żymankowska-Kumon, Holtzer, Olejnik & Bobrowski, 2012). The positive ions of the montmorillonite form diffuse ionic layers, resulting in electrostatic repulsions, but when heated, the clay particles agglomerate due to the reduction in the potential energy (Clem & Doehler, 1961). A gel structure gradually sets in, as particles assume minimum energy structures effected from the Brownian motion. While bentonite clays are very popular as binding media in traditional sand casting, there is no readily available literature on their applications in 3D printing. Considering their widespread use and time-tested attributes, it is interesting to investigate the possible use of the traditional bentonite and sand mixtures in 3D printing. The current research attempts this evaluating the mechanisms and mechanics of bonding with materials of varying compositions, while also allowing the superior thermal resistance and strength of bentonite at elevated temperatures (Hofmann, 1985) to be integrated into relatively simple mould material systems for 3D printing. The necessity of the present work is to identify the locally available bentonite-based sand materials suitable for use in a binder jetting printer. The objective of the current research is to assess the possibility of using traditional mould materials in 3D printing environment and to check the suitability of using such material system, and to assess the bonding mechanisms, in order to replace costly commercial material systems.

2. Materials System and Mechanism of Bonding

The current research is aimed to understand the mechanism of bonding of sand composites, and the mechanism of bonding in binder jetting is primarily dependent on the initiation and growth of gypsum crystals from the plaster component of the powder mixture (Bredt, Clark & Gilchrist, 2006). A certain amount of plaster is essential in the powder mixture, in order to achieve the necessary bonding and green strengths while implementing the 3D printing scheme. Both α and β-forms of hemihydrate possess properties suitable for this application. However, considering the mechanical strength, α-hemihydrate is selected for the purpose (Singh & Middendorf, 2007).

Accelerators of gypsum reaction are essential and literature suggests either pre-moisturisation (Yu & Brouwers, 2011) or addition of a certain quantity of di-hydrate (Bredt, Clark & Gilchrist, 2006) as possible means. In the current research, small quantities of terra alba, a commercial form of di-hydrate, is used as the seeding material. Preliminary trials employing different amounts of terra alba resulted in promising results in terms of green strengths achieved in the printed specimens. Figure 1 shows a schematic representation of the experimental workflow and Table 1 presents the basic ingredients of the mould material system used in experiments that follow. The compositions were identified based on *a priori* data generated from a number of repeated trials printing small rectangular specimens subjected to green strength evaluations.

The mechanisms of bonding achieved with varying compositions are first investigated in order to be able to assess the effectiveness of the materials composed for 3D printing. Photomicrographs of 3D printed green samples of varying compositions are presented in Figure 2. With terra alba and bentonite remaining at similar levels, the gypsum crystallisation generally increased with increasing α-hemihydrate from 25% to 75%. This is due to the availability of the plaster for a given amount of water added to the system (Yu & Brouwers, 2012). While the crystals are relatively shorter and kind of plastered around by bentonite at lower levels of hemihydrate, sharp needle-like crystals grew, forming intricate networks as the hemihydrate content increased, as may be observed on comparing photo micrographs of the first and the last rows in Figure 2, in pairs vertically. The role of terra alba is to promote formation of gypsum crystals (Martias, Joliff, Nait-Alib & Zabomiak, 2013). This is clearly evident on comparing the photomicrographs of Figure 2 (i) (a) and (d), (ii) (b) and (d), and (iii) (a) and (d); each pair representing the effects of increasing terra alba content, while the other contents remain at similar levels.

Table 1. The mould material system

S. No	Material	Chemical Formula	Supplier	Weight	% Level
1	Silica Sand (AFS fines No. 60 – 65)	SiO_2	Industrial Sands Ltd, NZ.	100%	100
2	USG Hydrocal FGR95	$CaSO_4$. $0.5H_2O$	United States Gypsum Company	50% of sand	25-75
3	Terra Alba	$CaSO_4$. $2H_2O$	Winstone Gypsum, NZ.	50% of α-HH	12.5 - 37.5
4	Calcium Bentonite	$Al_2O_3.4(SiO_2).H_2O$	Industrial Minerals (NZ) Ltd.	50% of Terra Alba	6.25-18.75

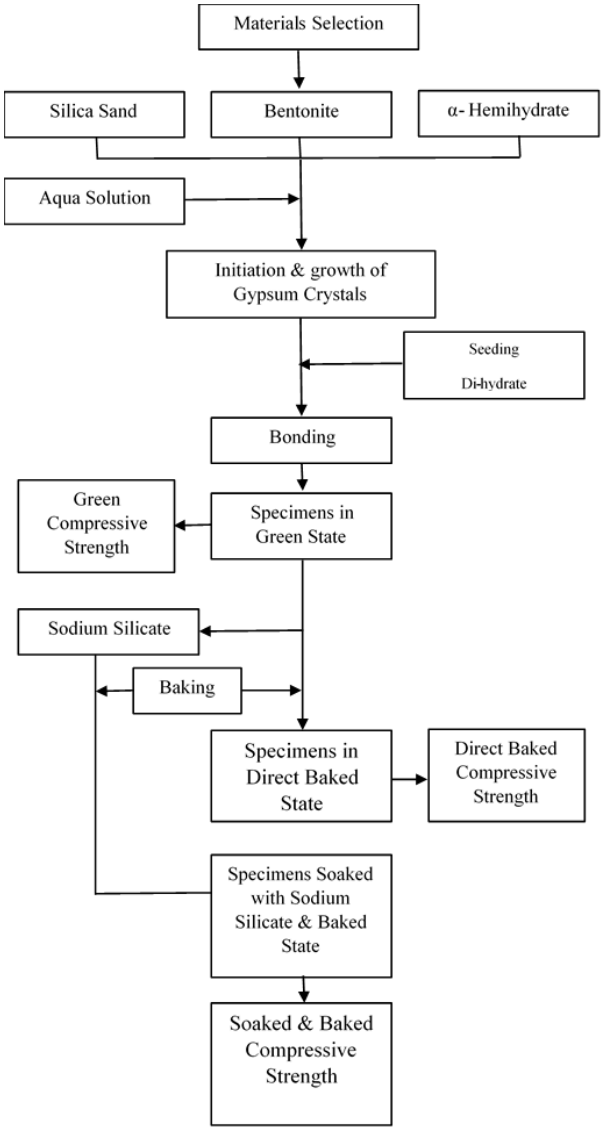

Figure 1. Schematic representation of experimental work flow

Cody and Shanks (1974) propose that gelling clays such as montmorillonite and Wyoming bentonite allow for large crystals of gypsum to grow. It was identified that bentonite resembles natural sediments in terms of promoting gypsum crystal growth. While it is to be accepted that the presence of bentonite allows gypsum crystal growth, it does not necessarily mean that the more there is bentonite, the higher is the growth of gypsum crystals; other ingredients such as hemihydrate are likely to interact. For example, it is clearly evident that the gypsum crystal growth considerably increased from Figure 2 (i.b) to (i.c) as the bentonite increased from 6.25% to 18.75% at the same level of terra alba and 25% of hemihydrate. This effect is less pronounced in Figure 2 (ii.a) and (ii.b) at 50% hemihydrate, while there is hardly any effect of increasing bentonite in the samples obtained with 25% terra alba and 75% hemihydrate.

3. The Sodium Silicate Treatment

Sodium silicate acts as a foundry binder through the ability to form bonds by a precipitated gel. The semi-solid substances bond sand grains into continuous 3D arrays. As explained by Owusu (1982), sodium meta silicate solutions are in equilibrium with silicate acid and its ions, polysilicic acid and the gel. The silicic acid under suitable pH conditions forms polysilicic acid. The polysilicic acid in turn transforms into a gel, which will eventually harden due to shortening of the Si-O-Si distances and build-up of the tension within each chain by a suitable mechanism. Due to dispersion and mechanical compacting, sodium silicate covering individual grains forms bonds between adjacent sand grains due to necking resulting from surface tension forces (Owusu, 1982)

The mechanical compaction factor is absent, but the soaking of the printed sand specimens for sufficient time allows wide dispersion of the binder within the matrix of sand particles stuck together by means of gypsum crystals and bentonite spread in between, cushioning other ingredients. Pure water could have resulted in a loss of the printed structure as excess moisture occupies inter-lamellar spaces, softening the gypsum (Singh & Middendorf, 2007). Considering that the sodium silicate is already in a gel like structure, the H_2O component can either promote further gypsum crystal growth as per Equation 1 or just leave the structure as it is.

$$CaSO_4 \cdot 0.5H_2O + 1.5H_2O \rightarrow CaSO_4 \cdot 2H_2O + \text{Heat} \quad (1)$$

(S.B. Selvaraj & Singmaneni, 2015)

Evidently, all the photomicrographs of Figure 3 showing the microstructures of 3D printed samples, soaked in sodium silicate solution and baked, show the original gypsum crystal and sand grain structure coated in a white layer of the glassy solidified gel. As noted by Owusu (1982) sodium silicate does not act as a structure filling mortar, but stretches at the contact points of adjacent sand grains, bridging them through necks formed due to surface tension and viscosity. Inter-granular bonding through necking and subsequent solidification is clear in some cases, such as in Figure 3 (i.b). In cases where there is already a fine needle-like growth of the gypsum crystals, the sodium silicate component helped by coating the crystals first and then providing overall strength through the formation of a network of inter-granular bonds. In cases where the original structure has short and compressed

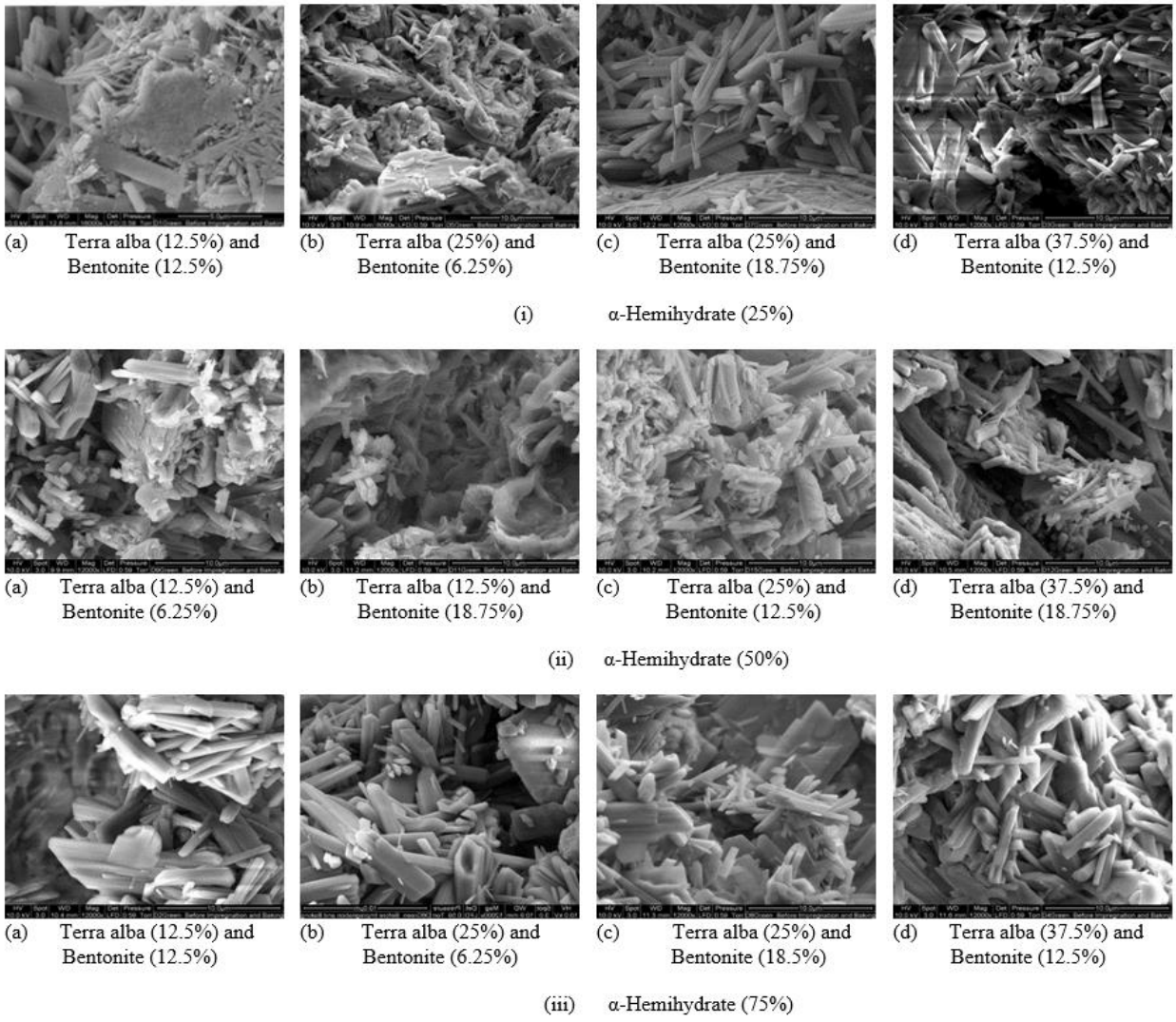

Figure 2. SEM photomicrographs of green samples 3D printed with varying compositions

gypsum crystals, the final resulting structure is predominantly constituted of a wide network of continuously distributed layer of solidified sodium silicate gel as observed in Figure 3 (ii.b and ii.c). Also, plate-like growth in the gypsum remained as coated plates, bonded inter-granularly in Figure 3 (ii.a), (iii.a), and (iii.c). Both needle-like and plate-like crystals are connected through intricate networks of vitrified sodium silicate bonds, compared to the widespread dispersion of the glassy gel matrix seen in Figure 3 (ii.b and ii.c). Presumably, the structures with wider network of solidified sodium silicate bonds could have achieved higher mechanical strengths than the other forms.

Overall, the sodium silicate treatment and the subsequent baking allowed the structural components of the mould material to be blanketed by the glassy substance resulting from the condensed siloxane bonds and the network of intergranular connections, the extent of which varies with the location.

4. Mechanics of Material Consolidation

In order to be able to understand the mechanics of bonding in 3D printed mould materials based on α-hemihydrate as the binder together with the other ingredients, a statistical design based on the Box-Behnken approach is chosen. This allowed three material factors; α-hemihydrate, terra alba, and calcium bentonite to be considered at three levels each and the general form of the regression models to be developed is given in Equation 2 to evaluate the variation of compressive strengths both in green and baked states are shown in Table 2.

$$Y = \beta_0 + \beta_1 X_1 + \beta_2 X_2 + \beta_3 X_3 + \beta_{11} X_1^2 + \beta_{22} X_2^2 + \beta_{33} X_3^2 + \beta_{12} X_1 X_2 + \beta_{13} X_1 X_3 + \beta_{23} X_2 X3 \quad (2)$$

(S. B. Selvaraj & Singmaneni, 2015)

where, β_0, β_1, β_2, β_3……..β_{23} – Coefficients, X_1 – α-hemihydrate, X_2 – Terra Alpha, X_3- Bentonite

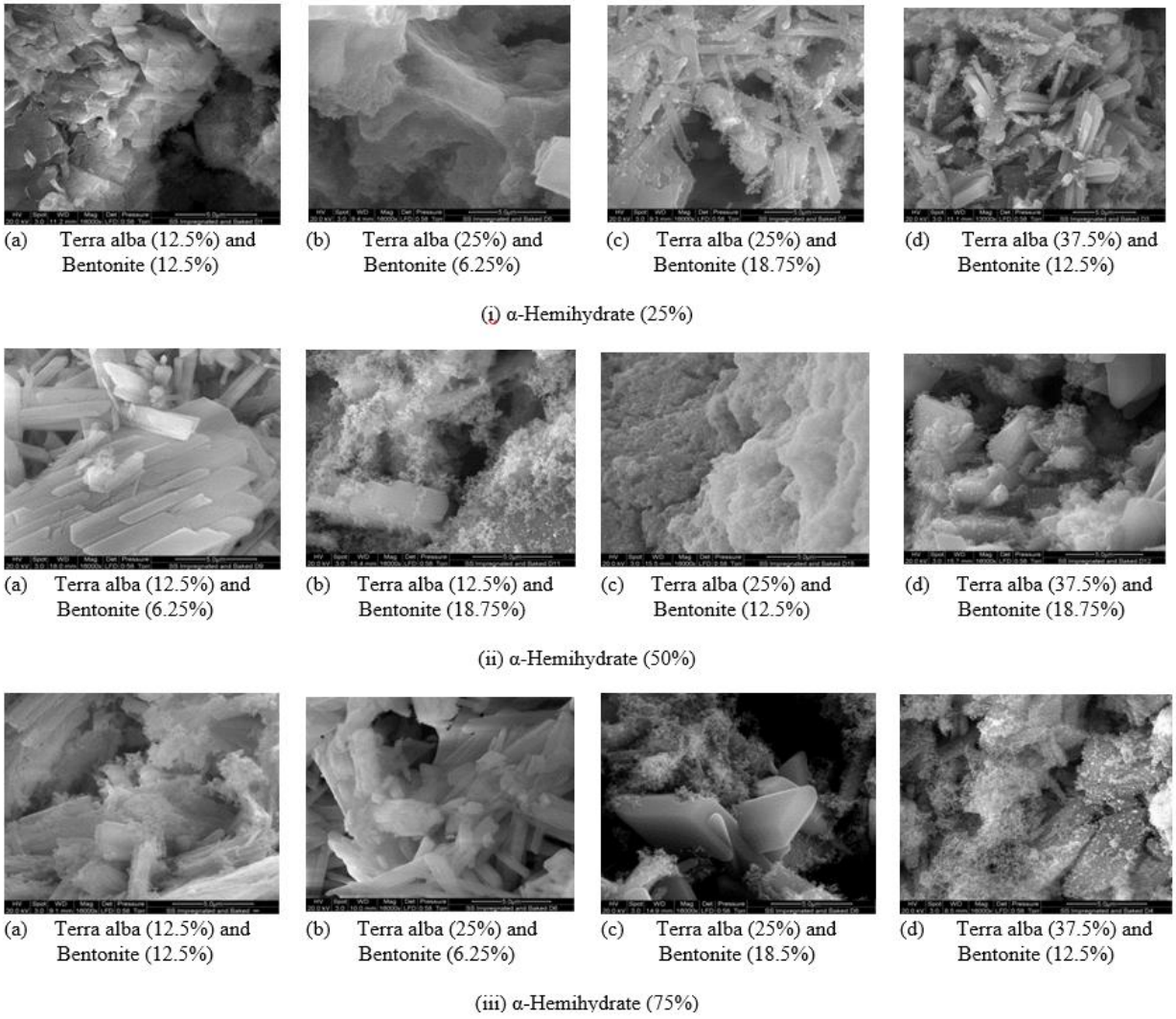

Figure 3. SEM photomicrographs 3D printed and sodium silicate soaked samples after baking

Table 2. Experimental design and observed responses

Run	α – HH	Terra Alba	Calcium Bentonite	Compressive strength (MPa)		
				Green	No impregnated & Baked	Impregnated & Baked
1	25	12.5	12.5	0.25	0.08	0.33
2	75	12.5	12.5	0.3	0.11	1.23
3	25	37.5	12.5	0.05	0.02	0.34
4	75	37.5	12.5	0.37	0.13	0.77
5	25	25	6.25	0.24	0.10	0.48
6	75	25	6.25	0.62	0.31	1.05
7	25	25	18.75	0.19	0.08	0.17
8	75	25	18.75	0.28	0.12	0.6
9	50	12.5	6.25	0.49	0.19	1.3
10	50	37.5	6.25	0.4	0.15	0.46
11	50	12.5	18.75	0.49	0.23	0.78
12	50	37.5	18.75	0.27	0.16	0.43
13	50	25	12.5	0.48	0.27	0.9
14	50	25	12.5	0.53	0.19	0.68
15	50	25	12.5	0.5	0.24	0.66

5. Compressive Strength

Compressive strength tests were conducted based on AFS standards using cylindrical specimens of size ϕ50 × 50mm and a Hounsfield Tensile Tester at the rate of 1 mm/min. The model from the experimental results for the green compressive strength is presented as Equation 3. Analysis of variance validated the model at 95% confidence level and the R^2 was 95.01% indicating that all variables are significant in controlling the variation of the response.

$$Y_{GCS} = - 0.6597669 + 0.0314106X_1 + 0.0196108X_2 + 0.0235895X_3 - 0.0002704X_{12} - 0.0005982X_{22} - 4.382E\text{-}05X_{32} + 0.0002215X_1X_2 - 0.0004566X_1X_3 - 0.0004009X_2X_3 \quad (3)$$

where Y_{GCS} is Compressive Strength in the green state.

Figure 4 presents the compressive strengths of the printed samples in green state for varying compositions. In almost all cases, the green compressive strength gradually increased, attained a peak and then reduced either substantially or to varying extents in other cases. Again, in the green state, the strength of the printed sample can be attributed to the nucleation, growth and final form of the gypsum crystals. As the percentage of α-hemihydrate increases, the crystal growth and gypsum bonding of the sand and clay masses increases, thus giving better compressive strength.

However, beyond a certain limit, the crystal growth is restricted by the amount of moisture available, while at the same time the unaltered plaster powder together with bentonite forms relatively softer zones promoting easier shear failure, resulting in a loss of compressive strength. Understandably, there is an optimum level of α-hemihydrate at around 50% which seems to be effective in developing the necessary bonds in the green state, for the amount of moisture added through the print head, and for each combination of the other parameters. Also, at higher terra alba and low to mid-range of bentonite contents, the compressive strength continuously increased with increasing hemihydrate. The terra alba promotes better seeding and relatively higher chances of the gypsum crystal growth with the moisture levels made available through the printing process. The regression model shown in Equation 4 is based on the compressive strength results of samples soaked in sodium silicate and baked. ANOVA validated the model at 95% confidence while R^2 at 92.13 % indicating all factors to be highly significant.

$$Y_{IBCS} = 0.2699548 + 0.0436652X_1 - 0.0314921X_2 - 0.0225901X_3 - 0.0001994X_1^2 + 0.0002829X_2^2 - 0.001264X_3^2 - 0.0003746X_1X_2 - 0.0002225X_1X_3 + 0.0015727X_2X_3 \quad (4)$$

where Y_{IBCS} is the Compressive Strength after impregnation and baking.

On soaking in sodium silicate and baking, the compressive strength generally increased with increasing α-hemihydrate. Figure 5 presents SEM photographs of baked samples showing evidence of increasing sodium silicate growth with increasing hemihydrate, with other conditions remaining the same, indicating continuous rise in the compressive strength. While variation in terra alba seems to have a relatively lesser influence, compressive strength after sodium silicate treatment and baking decreased to some extent with increasing bentonite. Lower α-HH (50%) together with the lowest Terra alba (12.5%) and Bentonite (6.25%) measured the highest green (144.7g) and baked (149.2g) masses also and resulted in the highest (1.3MPa) compressive strength in baked state as shown in Figure. 6.

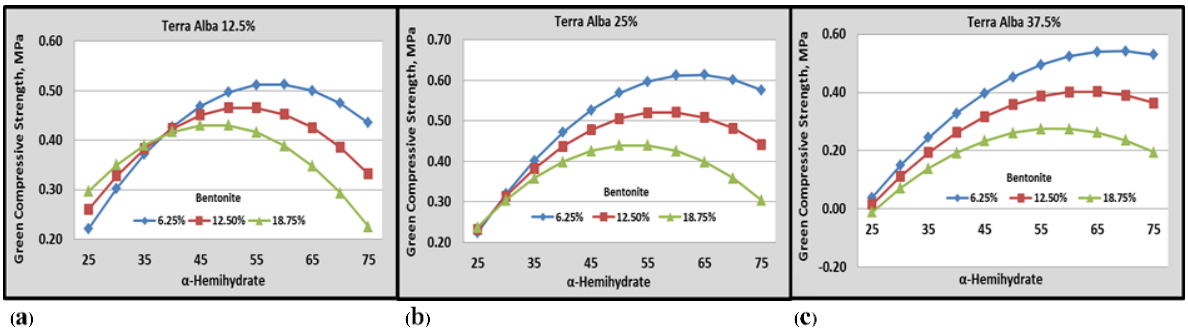

Figure 4. Variation in the green Compressive Strength with α-Hemihydrate content

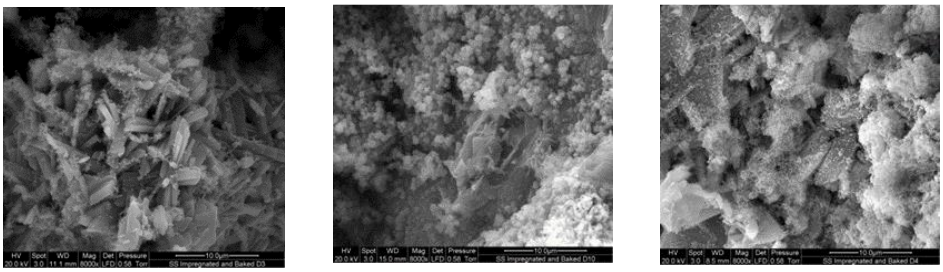

(a) α-Hemihydrate 25% (b) α-Hemihydrate 50% (c) α-Hemihydrate

Figure 5. Crystal structures post soaking and baking show increasing sodium silicate bonding with increasing α-hemihydrate at terra alba 37.5% and Bentonite 12.5%.

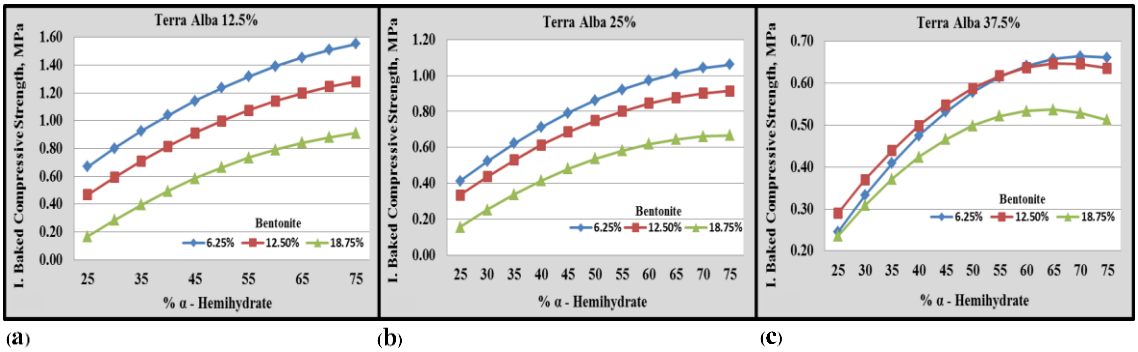

Figure 6. Variation in the compressive strength after sodium silicate soaking and baking with varying α-Hemihydrate content

Compressive strengths obtained in green, directly baked, and sodium silicate impregnated and baked states with all experimental combinations considered in the present work are plotted in Figure 7 for a direct comparison. It is clearly evident that direct baking after 3D printing resulted in almost negligible strengths for the specimens, while the sodium silicate treatment and subsequent baking worked well as a couple of the peaks are above the 1.0 MPa mark, indicating the suitability of the material system for casting a variety of metals, as per the standards of the American Foundry Society.

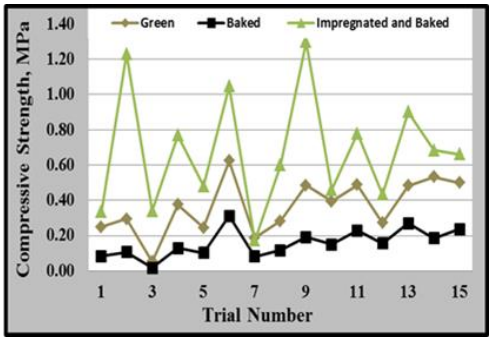

Figure 7. Comparative compressive strengths; green, directly baked, and sodium silicate impregnated and baked states

5. Conclusions

Notable differences could be observed on comparing the compressive strengths of three cases. Sodium silicate impregnation and baking resulted in the highest compressive strength for all the run compositions, as sodium silicate is a kind of resin which covered the sand particles and made strong necks linking the particles. Green compressive strength was higher due to moisture present in the samples, which was bonding in the green state. Direct dry compressive strength was lower; there was neither moisture nor resin bonding present to hold the particles, as water was almost completely driven off during baking and the departed moisture left pores and weak linking gave a lower strength.

Traditional foundry materials composed of bentonite and silica sand were tested for 3D printing of moulds and proved to be effective together with specific amounts of plaster and terra alba. The mechanism of bonding in green state is predominantly through gypsum crystallisation triggered by the plaster reacting to the moisture injected from the print head and assisted by terra alba as the seeding component. Sodium silicate soaking and impregnation are found to be essential and effective to achieve the required strength after baking, through inter-granular loading and crystal growth, apart from vitrified gypsum crystals. Sodium silicate treatment is effective in imparting post-baked strengths in 3D printed samples made of traditional foundry ingredients, but the nature and dispersion of the initial gypsum crystal growth will influence the overall results. Compressive strengths of green samples again showed a pattern with gradual increase, attaining a peak value, and then reducing with increasing α-hemihydrate at all levels of bentonite and terra alba, but the post-baked compressive strengths almost continuously increased with increasing plaster content. Overall, the optimum compressive strength required fixing α-hemihydrate at around 50-55% and terra alba at 12.5%, while compromises are possible with bentonite at 6.25% or 18.75% resulting in the most favourable compressive strength.

References

Bak, D. (2003). Rapid prototyping or rapid production? 3D printing processes move industry towards the latter. *Assembly Automation*, *23*(4), 340–345. doi:10.1108/01445150310501190

Boylu, F. (2011). Optimization of foundry sand characteristics of soda-activated calcium bentonite. *Applied Clay Science*, *52*(1–2), 104–108. doi:10.1016/J.CLAY.2011.02.005

Bredt, J. F., Anderson, T. C., & Russell, D. B. (2002). *U.S. Patent No. 6,416,850.* Washington, DC: U.S. Patent and Trademark Office

Bredt, J. F., Clark, S., & Gilchrist, G. (2006). *U.S. Patent No. 7,087,109.* Washington, DC: U.S. Patent and Trademark Office.

Chhabra, M., & Singh, R. (2011b). Rapid casting solutions: a review. *Rapid Prototyping Journal*, *17*(5), 328–350. doi:10.1108/13552541111156469

Chhabra, M., & Singh, R. (2012). Obtaining desired surface roughness of castings produced using ZCast direct metal casting process through Taguchi's experimental approach. *Rapid Prototyping Journal*, *18*(6), 458–471. doi:10.1108/13552541211272009

Chua, C. K., Feng, C., Lee, C. W., & Ang, G. Q. (2004). Rapid investment casting: direct and indirect approaches via model maker II. *The International Journal of Advanced Manufacturing Technology 2004 25:1*, *25*(1), 26–32. doi:10.1007/S00170-004-

1865-5

Clem, A. G., Doehler, R.W. (1961). Industrial Applications of Bentonite. *Clays and Clay Minerals*, 10(1), 272–283. doi:10.1346/CCMN.1961.0100122

Cody, R. D., & Shanks, H. R. (1974). A comparison of calcium sulfate dihydrate grown in clay gels and in sodium silicate gels. *Journal of Crystal Growth*, *23*(4), 275–281. doi:10.1016/0022-0248(74)90069-4

Drokina, V. V., Belov, V. D., & Chekhonin, S. N. (2011). Obtaining casts of aluminum alloys by foundry in loose molds fabricated on installations of three-dimensional printing. *Russian Journal of Non-Ferrous Metals 2011 52:1*, *52*(1), 24–28. doi:10.3103/S1067821211010081

Hofmann, F. (1985). Investigation on the Effect of Heat of the Bonding Properties of Various Bentonites, *AFS Transactions*, *66*, 377 – 384.

Gill, S. S., & Kaplas, M. (2010). Efficacy of powder-based three-dimensional printing (3DP) technologies for rapid casting of light alloys. *The International Journal of Advanced Manufacturing Technology 2010 52:1*, *52*(1), 53–64. doi:10.1007/S00170-010-2716-1

Kent, N. (1991). *Selective laser sintering as a rapid prototyping and manufacturing technique*. Retrieved from repositories.lib.utexas.edu/handle/2152/64328

Koltygin, A. V., & Bazhenov, V. E. (2012). Development of a substitute for Z cast molding sand used on installations of 3D printing for obtaining aluminum, magnesium, and iron casting. *Russian Journal of Non-Ferrous Metals 2012 53:1*, *53*(1), 38–41. doi:10.3103/S1067821212010129

Lee, C. W., Chua, C. K., Cheah, C. M., Tan, L. H., & Feng, C. (2004). Rapid investment casting: Direct and indirect approaches via fused deposition modelling. *International Journal of Advanced Manufacturing Technology*, *23*(1–2), 93–101. doi:10.1007/S00170-003-1694-Y

Mandal, P. K., & Mandal, T. K. (2002). Anion water in gypsum (CaSO4·2H2O) and hemihydrate (CaSO4·1/2H2O). *Cement and Concrete Research*, *32*(2), 313–316. doi:10.1016/S0008-8846(01)00675-5

Markowski, T., Budzik, G., Kozik, B., Dziubek, T., Sobolewski, B., & Zaborniak, M. (2010). Geometrical precision of 3DP casting form for founding gears. *Archives of Foundry Engineering*, *10*, 391–394.

Martiasa, C., Joliff, Y., Nait-Alib, B., Rogezc, J., & Favottoc, C. (2013). A new composite based on gypsum matrix and mineral additives: Hydration process of the matrix and thermal properties at room temperature. *Thermochimica Acta*, *567*, 15–26. doi:10.1016/J.TCA.2013.03.001

Mohammad Reza Khosravani, Tamara Reinicke, On the Use of X-ray Computed Tomography in Assessment of 3D-Printed Components, Journal of Nondestructive Evaluation (2020) 39:75, doi.org/10.1007/s10921-020-00721-1.

Owusu, Y. A. (1982). Physical-chemistry study of sodium silicate as a foundry sand binder. *Advances in Colloid and Interface Science*, *18*(1–2), 57–91. doi:10.1016/0001-8686(82)85031-8

Rosochowski, A., & Matuszak, A. (2000). Rapid tooling: the state of the art. *Journal of Materials Processing Technology*, *106*(1–3), 191–198. doi:10.1016/S0924-0136(00)00613-0

Simchi, A., Petzoldt, F., & Pohl, H. (2003). On the development of direct metal laser sintering for rapid tooling. *Journal of Materials Processing Technology*, *141*(3), 319–328. doi:10.1016/S0924-0136(03)00283-8

Singh, N. B., & Middendorf, B. (2007). Calcium sulphate hemihydrate hydration leading to gypsum crystallization. *Progress in Crystal Growth and Characterization of Materials*, *53*(1), 57–77. doi:10.1016/J.PCRYSGROW.2007.01.002

Solaman B. Selvaraj, Sarat Singamneni. (2015), Pre-Moisturised β-hemihydrate for 3D Printed Moulds, *Journal of Materials and Manufacturing Processes*, 31, (8), 1102-1112. doi:10.1080/10426914.2015.1037918

Strydom, C. A., Hudson-Lamb, D. L., Potgieter, J. H., & Dagg, E. (1995). The thermal dehydration of synthetic gypsum. *Thermochimica Acta*, *269–270*(C), 631–638. doi:10.1016/0040-6031(95)02521-9

Utela, B., Storti, D., Anderson, R., & Ganter, M. (2008). A review of process development steps for new material systems in three dimensional printing (3DP). *Journal of Manufacturing Processes*, *10*(2), 96–104. doi:10.1016/J.JMAPRO.2009.03.002

Yu, Q. L., & Brouwers, H. J. H. (2011). Microstructure and mechanical properties of β-hemihydrate produced gypsum: An insight from its hydration process. *Construction and Building Materials*, *25*(7), 3149–3157. doi:10.1016/J.CONBUILDMAT.2010.12.005

Yu, Q. L., & Brouwers, H. J. H. (2012). Development of a self-compacting gypsum-based lightweight composite. *Cement and Concrete Composites*, *34*(9), 1033–1043. doi:10.1016/J.CEMCONCOMP.2012.05.004

Żymankowska-Kumon, S., Holtzer, M., Olejnik, E., & Bobrowski, A. (2012). Influence of the Changes of the Structure of Foundry Bentonites on Their Binding Properties. *Materials Science*, *18*(1), 57–61. doi:10.5755/J01.MS.18.1.1342